Eur. Phys. J. Special Topics **224**, 3279–3293 (2015)

DOI: 10.1140/epjst/e2015-50235-9

THE EUROPEAN PHYSICAL JOURNAL SPECIAL TOPICS

Regular Article

A transfer entropy analysis of leader-follower interactions in flying bats

N. Orange and N. Abaid[a]

Department of Biomedical Engineering and Mechanics, Virginia Polytechnic Institute and State University, Blacksburg, VA 24061, USA

Received 7 August 2015 / Received in final form 2 November 2015
Published online 15 December 2015

Abstract. In this paper, we present a transfer entropy analysis applied to the 3D paths of bats flying in pairs. The 3D trajectories are one-dimensionally characterized as inverse curvature time series to allow for entropy calculations. In addition to a traditional formulation of information flow between pair members, a path coupling hypothesis is pursued with time-delay modifications implemented in such a way as to not change the Markovianity of the process. With this modification, we find trends that suggest a leader-follower interaction between the front bat and the rear bat, although statistical significance is not reached due in part to the small number of pairs considered.

1 Introduction

Bat navigation and group dynamics represent a rich subject area of potential study. Highly evolved collective motion utilizing active sensory echolocation creates numerous avenues of exploration that can benefit our understanding of swarming mechanics, consensus modeling [1], collective robotics [2,3], and optimization strategy [4,5]. In recent years, significant progress has been made in capturing the fundamental phenomena involved in these natural systems. Evidence of frequency modulation capabilities show that bats have evolved echolocation behaviors to mediate their interactions with conspecifics [6,7]. Similar behaviors include vocalization cessation [8], which can allow bats to switch from active to passive sensing, and even offensive jamming during feeding competition [9]. These behaviors evidence that bats act differently together than alone.

Modern agent-based swarm modeling and consensus modeling can provide some additional insight towards understanding the complexity of bat group motion. Particularly salient lessons are the importance of goal-orientation and leadership [10,11]. While we can observe and understand the navigational goals of bat agents, such as feeding or energy conservation, clearly defining navigational leadership roles, even relative ones, in real systems is a challenge. In particular, a quantitative assessment of navigational leadership within bat groups appears to be an entirely untouched

[a] e-mail: nabaid@vt.edu

area of study. Given the broadcast nature of bio-sonar, the active sensing of one individual can directly influence the motions of others, making the directionality of leadership unclear.

In this paper, we contribute to the understanding of navigational leadership in bats. We refine our exploration of this area by focusing our efforts on pairs of bats and pursue a method of analysis involving the application of transfer entropy. Transfer entropy is a measure of directional information transfer between random processes. Centered around the concept of Shannon entropy [12,13], transfer entropy allows pairs of time series to be assessed in terms of the strength and direction of their coupling [14–16] by measuring the reduction in uncertainty of one time series when knowledge of the other time series is gained. With rapidly increasing interest, transfer entropy has been successfully applied to a large variety of subject areas including neuroscience [17], economics [18], and social media [19]. Notably, entropy approaches have been developed for assessing animal behavior and animal-robot interactions [20–23] and information transfer in swarming models [24].

This wide base of information-theoretic literature provides us with an excellent foundation with which to structure a novel approach to the problem of bat navigational leadership. Our core concept is to apply a transfer entropy analysis to characteristic kinematic time series representing the 3D paths of bats flying in pairs. Differing values of directional transfer entropies between members of each pair are expected to evidence potential leadership roles.

We collect and examine the 3D trajectories of wild bats flying in pairs; we find qualitative evidence that a coupling between their paths appears. This finding is notable since we collect data in a controlled cave environment which is consistent through time and, although a large variety of path shapes are displayed, the paths of the bats within a pair are qualitatively similar. Thus, the hypothesis of a path coupling within pairs is tested in this paper. A cursory examination of the simultaneous inverse curvature plots also supports this hypothesis. Strong curvature equivalency can be detected in many pairs, though the equivalency occurs across a significant time delay, a phenomenon that is explored in this work.

With these observations, we believe directional information transfer exists within the bat pairs and that this interaction is demonstrated by path shapes. Though the direction and magnitude of path coupling is not obvious from examining bat flight paths, we hypothesize that we can resolve these properties using a transfer entropy analysis of the inverse curvature time series or other kinematic metrics.

After applying a modified entropy formulation that allows us to capture the time delay inherent with path coupling, we calculate directional transfer entropy values for each pair. We find higher information transfer from the bat flying in front to the bat flying in the rear when we consider the path coupling time delay, as compared to all other entropy transfer figures (front to rear with no time delay, rear to front, and random pair shuffling); these trends fail to reach statistical significance due to the small number of bat pairs considered. Nevertheless, this result provides evidence that relative spatial positioning plays an important role in navigational leadership and quantifies the amount of path coupling that occurs within interacting pairs of flying bats.

2 Data collection and post-processing

We collected our data in a mountain cave in Jinan, China, in which, a long, hallway-like portion of the cave was found to be ideal for tracking continuous paths of small groups of bats. A 3D near-infrared camera system was setup and calibrated to obtain the 3D paths of bats along a 12 meter portion of the cave "hallway." This camera

Fig. 1. Infrared vision image of the field site in Jinan, China. The purple hue represents the 950 nm near-infrared wavelength interpreted by the GoPro camera's IR-sensitive hardware.

Table 1. General flight trajectory data.

Pair	Flight path type	Front bat avg vel (m/s)	Rear bat avg vel (m/s)	Avg separation (m)	Δt (s)
1	Straight through	6.28	6.16	2.94	0.48
2	Straight through	5.05	5.93	2.93	0.49
3	Turn back	3.11	2.60	1.13	0.44
4	Straight through	4.00	4.74	4.37	0.92
5	Straight through	4.98	5.48	2.49	0.45
6	Straight through	4.72	5.26	3.48	0.66
7	Straight through	5.76	5.01	3.16	0.63
8	Straight through	6.58	5.90	3.37	0.57
9	Turn back	4.44	5.49	2.69	0.49
10	Straight through	5.33	3.78	3.05	0.81

system consisted of 6 modified GoPro cameras filming at 1920×1080 resolution and 60 Hz. 950 nm LED arrays were used to create artificial illumination that is invisible to the natural eye, but able to be detected by the modified camera hardware, as shown in Fig. 1.

Intrinsic camera calibration was performed with the Caltech Camera Calibration Toolbox [25] for MATLAB software (The MathWorks, Inc., Natick, MA, USA) and spatial calibration with the Svoboda Multi-Camera Self-Calibration method [26]. Image processing and 3D reconstruction were performed with custom MATLAB codes following well-established triangulation techniques. A detailed description of the experimental setup and data processing can be found in [27].

We manually tracked ten pairs of bats as they flew through the volume. Pairs were selected if two bats coincided in the tracking volume for 50 or more frames and no other bats were in the tracking volume throughout the duration of the pair's flight. The purpose of this measure was to best enforce that the two bats being tracked were only interacting with each other, rather than surrounding bats. Some bats flew directly through the hallway, while others made a complete turning maneuver and returned the direction they came. In all cases, the first bat to enter the tracking volume was labeled as the front bat, and the other, the rear bat. Details of the tracked paths are shown in Table 1.

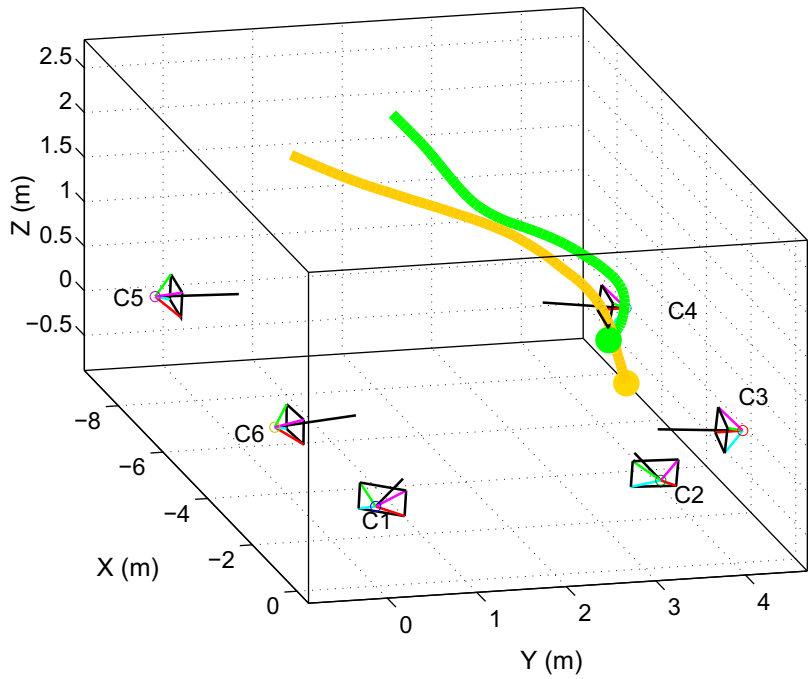

Fig. 2. A 3D reconstruction of the complete paths made by Pair 2. The green path represents the front bat and the yellow path the rear bat. The 6 camera positions, orientations, and fields of view are also represented. Note the similarity of the path shape. Other pairs display comparable similarity.

The 3D path points of each bat were extracted from the video data and a first-order locally weighted smoothing method was applied using the "lowess" built-in function in MATLAB. This method eliminates residual tracking error and oscillatory motion of the bat's centroid resulting from wing beat, while best considering the fundamental linear momentum of a flying bat. A sample of these 3D paths is shown in Fig. 2.

Although a transfer entropy analysis of these pairs can be computed for the three-dimensional signals, this would require a very large number of data points to build sufficiently dense probability distributions for the analysis. Hence, we generated one-dimensional time series from three-dimensional path data. We considered a number of potential metrics for representing 1D time series and found that an inverse radius of curvature metric was best for a number of reasons. Primarily, a curvature-based time series would be reflective of a bat's steering and thereby provide a good depiction of the 3D navigation of the bat pairs. Secondarily, an absolute inverse radius of curvature formulation would ensure the data remains positive and close to zero, making a logarithmic binning strategy possible. Finally, inverse radius of curvature was sufficiently time-varying to be a good candidate for entropy analysis without being as chaotic as a higher-order metric, such as kinematic jerk. As an additional reason, curvature-based metrics are frequently used to assess the motion of interacting agents, such as in the study of laboratory insects [28]. Nevertheless, we do perform entropy analyses on other metrics, as presented in the results section of this paper.

To extract the inverse radius of curvature time series, we first fit a third-order spline through the 3D path points and re-sample in time at the desired sample rate, if different than the original 60 Hz. We then differentiate the spline twice to generate 3D velocity $\mathbf{v} \in \mathbb{R}^3$ and acceleration $\mathbf{a} \in \mathbb{R}^3$ at each point in inertial coordinates.

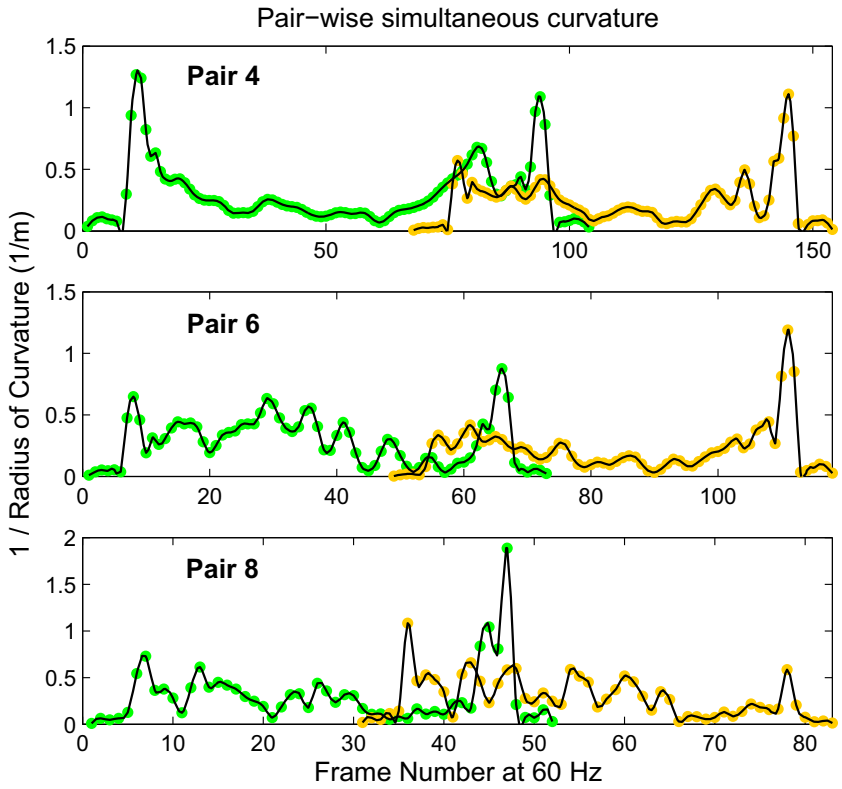

Fig. 3. Sample pair-wise inverse curvature time series occurring in real time, as per the camera frame number. The green curve represents the front bat and the yellow curve the rear bat. It is critical to note, again, the similarity in shape. The time-delay, demonstrated by the x-axis displacement between each curve pair, can be accounted for with the modified transfer entropy formulation.

The acceleration can be decomposed into components normal and tangential to the flight path ($\mathbf{a_n} \in \mathbb{R}^3$ and $\mathbf{a_t} \in \mathbb{R}^3$, respectively), as follows:

$$\mathbf{a_n} = \mathbf{a} - \mathbf{a_t} = \mathbf{a} - \frac{\mathbf{a} \cdot \mathbf{v}}{\|\mathbf{v}\|^2}\mathbf{v}. \tag{1}$$

The normal acceleration is used to determine the inverse radius of curvature ($1/R$):

$$\frac{1}{R} = \frac{\|\mathbf{a_n}\|}{\|\mathbf{v}\|^2} \tag{2}$$

Figure 3 shows sample plots of the calculated inverse curvature time series pairs.

As a validation of this method, we performed a discrete calculation of spatial curvature taken from Bergou [29] and found that the two methods displayed identical trends but with different proportional scaling as a result of dimensional differences. We elected to keep the spline-differentiation method because it retained a 1/m unit scale, which was useful for interpretation.

To achieve the discretized time series data necessary for entropy analysis, a straight-forward logarithmic binning strategy was employed. Bins ranges were logarithmically spaced from $10^{-1.3}$ to $10^{0.4}$ m^{-1}, these values being representative of nominal minima and maxima of the data set. Exceptional points that were less than

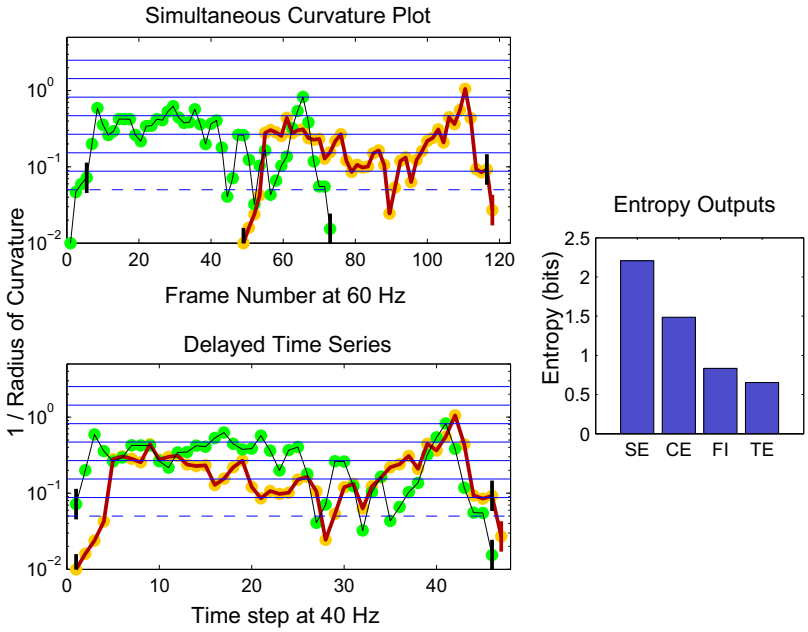

Fig. 4. Depiction of the modified Markov process. The top plot displays the original curvature time series from Fig. 3, having been down-sampled (sub-frame timing is applied as necessary) and placed on a log scale. The lower plot displays the truncated and shifted time series with respect to the locally defined time step. In both plots, the green dot signal represents the front bat and the yellow dot signal the rear bat. The signal highlighted in red is the entropy recipient, $\mathbf{x}$, for which the entropy values are being calculated; in this case, the entropy recipient is the rear bat. The non-highlighted signal is the entropy source, $\mathbf{y}$. Blue horizontal lines represent the minimum of each binning zone, eight in total. The lowest line is dashed since the lowest bin includes all values below its stated minimum. The unused bins have no effect on entropy calculations and are used by other pairs. The probability distributions generated by this example are shown in Fig. 5. Looking at the entropy recipient, the red vertical line marks the final value of $\mathbf{x}$, while the black vertical lines mark the first and last value of $\mathbf{x_p}$. Similarly, looking at the entropy source, the black vertical lines mark the first and last value of $\mathbf{y_p}$, given the imposed n. Moving from the top plot to the bottom, we see the black vertical lines line up in time, indicating that these previously separated points (and all points in between) are being correlated in the calculation of free information $H(\mathbf{x}|\mathbf{x_p}, \mathbf{y_p})$, as per the modified formulation. All data presented here is sourced from Pair 6 at a sample rate of 40 Hz, $n = 30$ time steps. Though it is not relevant to the final analysis, for clarity, calculated entropy outputs (Shannon entropy: SE, conditional entropy: CE, free information: FI, transfer entropy: TE) for this example are given in the bar plot on the right.

$10^{-1.3}$ m^{-1} were grouped into the lowest bin. A logarithmic scale was adopted to distribute data points more uniformly throughout the bins, since curvatures followed an approximate power law distribution. A plot depicting this binning strategy is shown in Fig. 4 and the resulting probability distributions used in entropy calculations are shown in Fig. 5.

3 Transfer entropy approach and hypothesis testing

To prove our hypothesis of path coupling, we perform a transfer entropy analysis of the inverse curvature data. With a one-dimensional, discretized time series, we

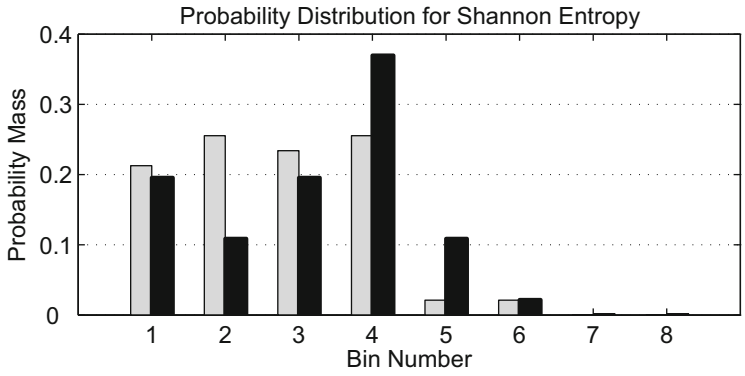

Fig. 5. Sample plot of the probability distributions generated by the fixed logarithmic binning strategy employed on the curvature data, to be used in the calculation of Shannon Entropy. The gray and black bars are the probability distributions of the $\mathbf{x}$ and $\mathbf{y}$ time series used in Fig. 4.

first apply a straightforward Shannon transfer entropy formulation [12,30]. Shannon entropy, conditional entropy and free information are given by Eqs. (3), (4), and (5), respectively:

$$H(\mathbf{x}) = -\sum_{\mathbf{x}\in A} p(\mathbf{x}) \log p(\mathbf{x}) \tag{3}$$

$$H(\mathbf{x}|\mathbf{x_p}) = -\sum_{\mathbf{x},\mathbf{x_p}\in A} p(\mathbf{x},\mathbf{x_p}) \log p(\mathbf{x}|\mathbf{x_p}) \tag{4}$$

$$H(\mathbf{x}|\mathbf{x_p},\mathbf{y_p}) = -\sum_{\mathbf{x},\mathbf{x_p},\mathbf{y_p}\in A} p(\mathbf{x},\mathbf{x_p},\mathbf{y_p}) \log p(\mathbf{x}|\mathbf{x_p},\mathbf{y_p}). \tag{5}$$

The time series $\mathbf{x}$ and $\mathbf{y}$ are the entropy sink and source, respectively. In other words, they are discrete-valued vectors of two inverse curvature signals from two different bats where we are testing whether the bat $\mathbf{x}$ (sink) receives information from bat $\mathbf{y}$ (source). The set A represents the possible discrete values of $\mathbf{x}$ and $\mathbf{y}$, as determined by the number of bins k, such that $A = \{a_1, a_2, ...a_k\}$. The shifted time series $\mathbf{x_p}$ and $\mathbf{y_p}$ are the preceding values of $\mathbf{x}$ and $\mathbf{y}$, respectively, that is, the series shifted by one time step. The function $p(\mathbf{x})$ represents the probability distribution of $\mathbf{x}$, determined by the frequency of a symbol ($a_i \in A$) appearing in the $\mathbf{x}$ time series. The distributions $p(\mathbf{x},\mathbf{x_p})$ and $p(\mathbf{x}|\mathbf{x_p})$ represent the digram and transitional probability distributions, respectively, of the $\mathbf{x}$ time series. Similarly, $p(\mathbf{x},\mathbf{x_p},\mathbf{y_p})$ and $p(\mathbf{x}|\mathbf{x_p},\mathbf{y_p})$ represent the digram and transitional probability distributions, respectively, of the $\mathbf{x}$ time series, with knowledge of the $\mathbf{y}$ time series.

In this way, conditional entropy indicates the total information of $\mathbf{x}$ given the previous values of $\mathbf{x}$, while free information represents the information of $\mathbf{x}$ given the previous values of $\mathbf{x}$ and $\mathbf{y}$. Thus, transfer entropy can be calculated in Eq. (6), where transfer entropy is the information of $\mathbf{x}$ coming from previous values of $\mathbf{y}$ but not previous values of $\mathbf{x}$.

$$TE(\mathbf{y} \to \mathbf{x}) = H(\mathbf{x}|\mathbf{x_p}) - H(\mathbf{x}|\mathbf{x_p},\mathbf{y_p}). \tag{6}$$

We assume that this information transfer is governed by a 1st order Markov process [12], in which current values of a signal are only affected by the values of

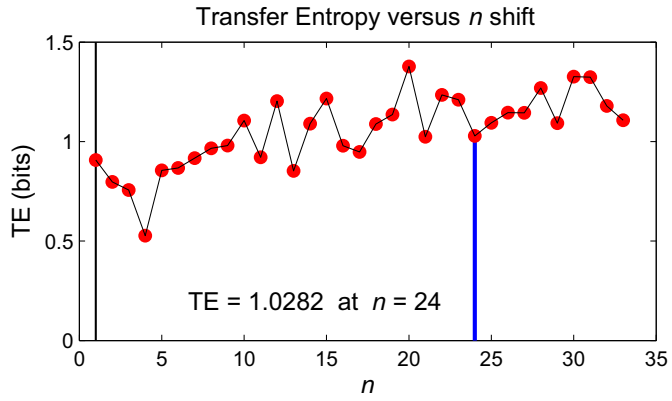

Fig. 6. Sample plot of the general effect of n on transfer entropy. Generated from Pair 8 at 40 Hz with ten bins. The blue line represents the TE value of this data at $n = 24$, the n shift value calculated with the $\Delta t = 0.57$ value for Pair 8, using Eq. (7).

a single previous time step. In accordance with the properties of this assumption, a number of important concepts are developed.

First, we must intelligently sample our curvature data such that a stimulus-response cycle can occur within a single time step. If the bats are not capable of observing and adjusting their trajectory within a single time step, positive results cannot be expected. This is resolved with a characteristic time scale argument later in this paper.

Secondly, if interaction is delayed (in that a bat is capable of making a trajectory adjustment in a single time step, but waits until later time steps to do so), a 1st order Markov formulation conditioning on the immediately previous time step will not produce positive results. Based on the path coupling hypothesis and the time delay we see in the simultaneous inverse curvature plots, we anticipate encountering an interaction delay of this kind. This leads us to develop a method for addressing and capturing this potential phenomenon.

Hence, a modified 1st order Markov process is proposed. We adjust our calculation of free information in Eq. (6) such that $\mathbf{y_p}$ encapsulates the value of the entropy source signal at n time steps in the past ($t - n$, where $n \geq 1$). This formulation maintains the 1st order Markovianity of the process because the entropy recipient can still only refer to a single previous state of the entropy source, though that state is now n time steps preceding, instead of just one time step preceding. Conceptually, this is equivalent to a bat detecting an important change in his partner's path immediately, but consistently waiting until a later time step to incorporate that change, as would be the case for a bat that is attempting to follow another bat that is substantially ahead (in front). The final process is similar to methods for studying time-delayed dependencies that have been developed in well-established literature [15]. Figure 4 serves to illuminate the function of the modified Markov process. Additionally, a plot of the effect of n on a single transfer entropy calculation is shown in Fig. 6.

With this modified formulation, we create an additional variable in our calculations of transfer entropy, n. To visualize the interactions of all three variables (number of bins, sample rate, and n shift value), we can plot a 2D transfer entropy map that varies sample rate and n shift. These maps can be generated for any number of bins, any pair, and any direction of interaction. Some samples of these maps are shown in Fig. 7.

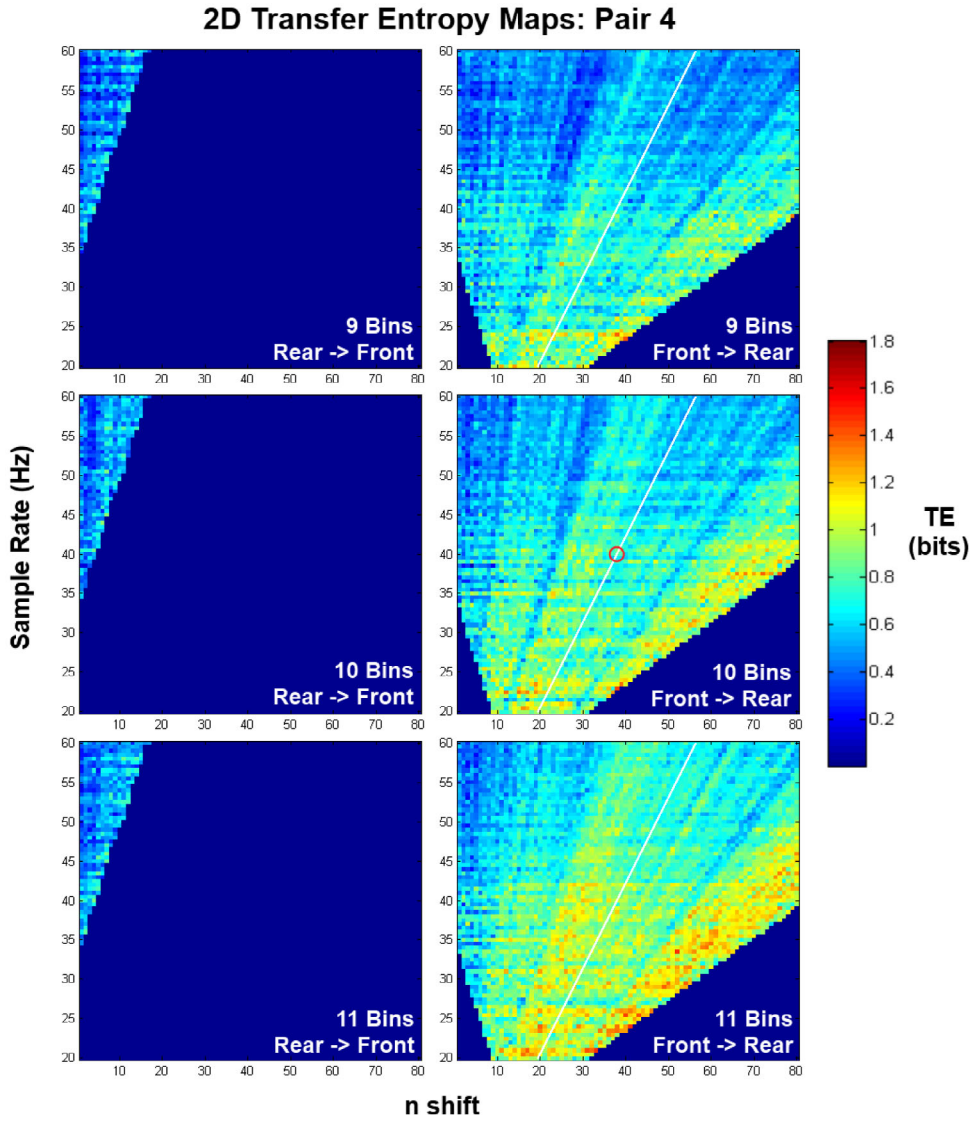

Fig. 7. Sample of 2D transfer entropy maps. With axes of n shift and sample rate, variables such as pair number, directionality, and number of bins can be varied. Here, number of bins is varied from 9 to 11 considering both directions of information transfer in Pair 4. The thin white lines represent the Δt value for Pair 4 projected onto the front to rear maps using Eq. (7). The three red circles indicate entropy values used in the final analysis. Plot areas of zero TE lack sufficient points for entropy analysis. Front to rear direction plots cover a broader plot area because n shift increases the number of common points between each signal in this case; the opposite is true for the rear to front direction.

This huge array of transfer entropy data can be hazardous. Because results can depend strongly on the interpretation used, there are many opportunities for spurious conclusions to be reached [31]. In order to compose a supportable argument, we select a sample rate, number of bins, and time delay values that are physical reasonable,

such that they could be considered characteristic scales of the system. By doing this, we eliminate regimes of results that do not have physical meaning and we avoid the bias of selecting regimes that artificially provide the most positive results.

Given that an average wing-beat frequency for bats of the size we observed is 10 Hz [32] and that microchiropteran bats have been shown to emit four echolocation pulses per wing-beat [33], we select 40 Hz as a best guess of a physical characteristic time scale. This also allows us to address the issue of insufficient stimulus-response cycle time, mentioned previously.

The upper and lower limits of the bins used to count the data were chosen to guarantee that the observed maxima and minima of the bats' time series were accommodated. The number of bins was selected in accordance with the time step and characteristic bat velocity and acceleration, so that an individual was likely to occupy different bins over successive time steps. Based on these criteria, ten bins was found to be appropriate.

For the n shift values, we first calculate transfer entropy with the conventional $n = 1$ to see the standard values. However, as previously mentioned, we also hypothesized a time delay phenomenon correlating with path coupling. To capture this, we calculate a differential time factor (Δt) for each pair of bats as the ratio of the average distance between the front and rear bat and the average velocity of the rear bat. This differential time factor represents the average time lag between when the rear bat senses the front bat at a particular location and when the rear bat achieves an equivalent location along its own path. Effectively, this delay incorporates path information from the front path at an equivalent point in space, rather than the previous point in time. If we see increased value of transfer entropy using this shift, it will serve as evidence for a path-coupling behavior from the front bat to the rear bat and a leader-follower interaction. We comment that alternative methods of determining time shift are well-established in the literature [34,35]. However, these methods rely on using the time shift parameter to directly optimize transfer entropy. As a result, our method, which we prefer due to its behaviorally-based nature, is an inherently more conservative strategy.

Precise differential time values are given in Table 1 and can be converted into n shift values with Eq. (7), where SR is the chosen sample rate and rnd($\bullet$) rounds real numbers to the nearest integer.

$$n = \mathrm{rnd}(\Delta t \cdot SR) + 1. \tag{7}$$

It is critical to note that this delay factor is inherently directional from the front bat to the rear. Given that the front bat is exclusively in front of the rear bat and cannot perceive stimuli from future time steps, imposing this same shift for the rear to front interaction would be entirely non-physical and would require using a negative n value. Moreover, we comment that the selection of the delay factor can also be defined in terms of the volume sensed by the bats, effectually translating the spatial translation of tandem flight into a temporal shift. However, for this work, we avoid such assumptions since the video data does not allow for measuring the directionality of the bats' sensing organs, and thus their sensing volumes.

Based on these properties, we propose that the front bat is only able to receive and incorporate path information from the rear bat based on the previous time step, as per an unshifted 1st order Markov formulation, where as the rear bat can incorporate path information from front bat based on the previous time step or an equivalent point in space as per the $\Delta t \to n$ shift. This may seem to provide an unfair advantage to the rear bat, but this advantage appears to be inherent with nature of the system.

With all state variables decided, we calculate the final transfer entropies for each pair with each of these interaction modes to evaluate their respective presences. To clarify, the modalities we consider are: $RF_{n=1}$, entropy from the rear to the front bat

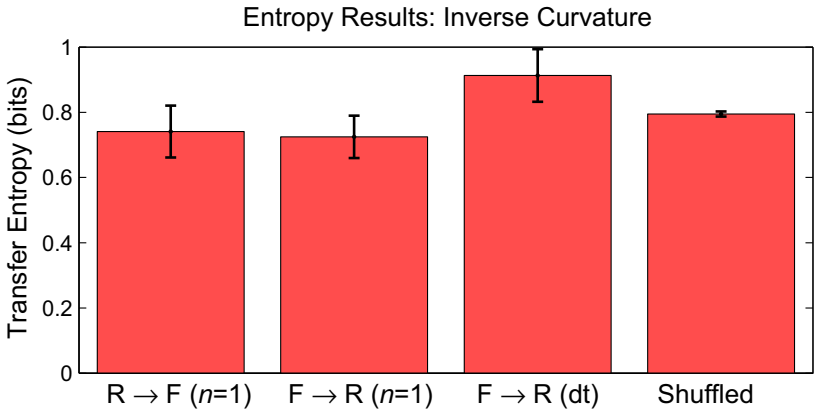

Fig. 8. Final transfer entropy results for all pairs in each modality at a sample rate of 40 Hz and with ten bins. Red bars represent sample means and black brackets indicate standard error. $N = 10$ pairs are used for the first three modalities and $N = 1000$ samples for the shuffled control modality. No significant differences in means are present.

with $n = 1$, $FR_{n=1}$, entropy from the front to the rear bat with $n = 1$, and $FR_{\Delta t}$, entropy from the front to the rear bat with n determined by Δt.

In addition to these three modalities, we add a fourth value representing a control condition, Modality Sh. Because there can be some amount of calculable information transfer between two time series that are entirely independent, we calculate the level of entropy present between curvature time series of bats that cannot possibly be interacting since they occupy the tracking volume at vastly different times. We accomplish this by randomly selecting 1000 sets of curvature time series, each set having an entropy recipient and source from different pairs, and calculating directional transfer entropy with a random n shift value. Ideally, this method can add validity to our results by representing a "background" level entropy that is systemic with our data and that other entropy levels can be compared to. Most importantly, matched pair modalities ($RF_{n=1}$, $FR_{n=1}$, and $FR_{\Delta t}$) need to exhibit higher levels of transfer entropy than the unmatched shuffled pair modality (Sh) in order to be considered significant.

4 Results

The results of our analysis can be seen in Fig. 8. As evidenced by the figure, the mean value of the front to rear with imposed delay modality ($FR_{\Delta t}$) is higher than all other modalities, which are roughly equal. Using JMP 11 software, we perform a one-way analysis of variance to test the statistical significance of these trends. Using a typical significance level of $p < 0.05$, we found no main effect of modality on the mean transfer entropies.

With a Tukey-Kramer HSD test performed for post-hoc, pairwise tests (JMP 11), we see that tests comparing Modality $FR_{\Delta t}$ to Modalities $RF_{n=1}$, $FR_{n=1}$, and Sh have lower p values (0.30, 0.38, 0.44, respectively) than all other pairs (0.77 for Sh to $FR_{n=1}$, 0.87 for Sh to $RF_{n=1}$, and 0.99 for $RF_{n=1}$ to $FR_{n=1}$). Although these tests fail to indicate statistical significance, the trend suggests that Modality $FR_{\Delta t}$ is the most dominant modality of directional information transfer in the system. This is to say, we find highest information transfer from the bat flying in front to the bat flying in the rear while considering the path coupling time delay. This result suggests that:

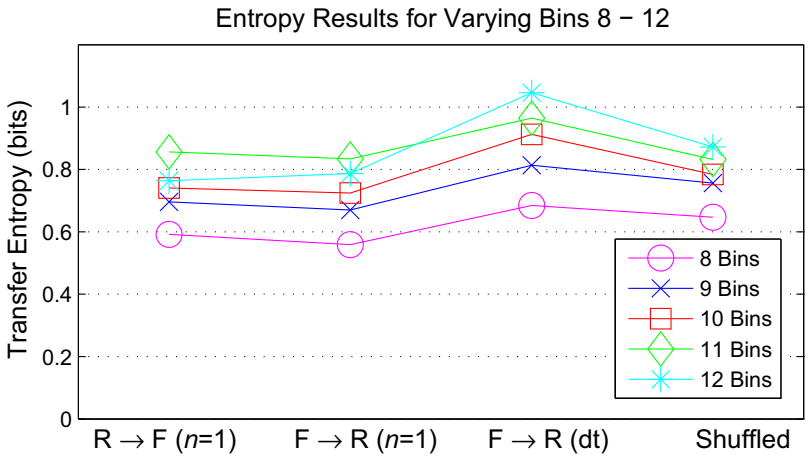

Fig. 9. Binning sensitivity plot for transfer entropy calculations using curvature data at 40 Hz. Though average transfer entropy tends to increase with an increased number of bins, the inter-modal trends are quite stable. This provides good evidence that sensitivity to number of bins is not an issue in the results presented in Fig. 8.

1) relative spatial positioning plays an important role in navigational leadership, 2) the front bat in particular fulfills a leadership role for the pair as a whole, and 3) the rear bat displays path coupling behavior with the leading bat.

The sensitivity of this analysis to the number of bins selected is of interest. To test this sensitivity, the final four-mode results in Fig. 8 using 10 bins are plotted against that of using 8, 9, 11, and 12 bins, shown in Fig. 9.

As mentioned in earlier parts of this paper, we do perform transfer entropy analyses on tangential acceleration and total acceleration metrics, alternatives to the inverse curvature metric we focused on. Though the data preparation section of this paper detailed why these metrics are not the best representations of bat motion or the best candidates for entropy calculations, the analyses of these metrics are fundamentally identical to the analysis of the inverse curvature metric; the only difference is a centered, linearly-spaced binning strategy for the alternative metrics rather than a fixed logarithmic strategy. Results for the tangential acceleration and total acceleration metrics are shown in Fig. 10. We see that TE values are consistently lower and trends are less noticeable than in Fig. 8, making these results less useful in addition to being less reliable. Given these observations, we choose to focus on the application and results of the inverse curvature metric.

5 Discussion

Given the statistical non-significance of our results, we cannot conclusively determine the dominant leadership structure of the bats we observed. Despite this, the general conclusions mesh well with predictions drawn from literature. Given our understanding of cessation in bat echolocation [8] and information cascades in swarming simulations [24], a position-based leadership structure with path coupling appears reasonable, lending some legitimacy to our conclusions. We suspect that in future studies with a larger sample size of pairs, the lack of significance we encounter may be rectified and a leadership structure can be clearly defined. In fact, a sample size analysis using the statistics of this data suggests that $N = 12$ rather than $N = 10$ would give a result with power 95% [36].

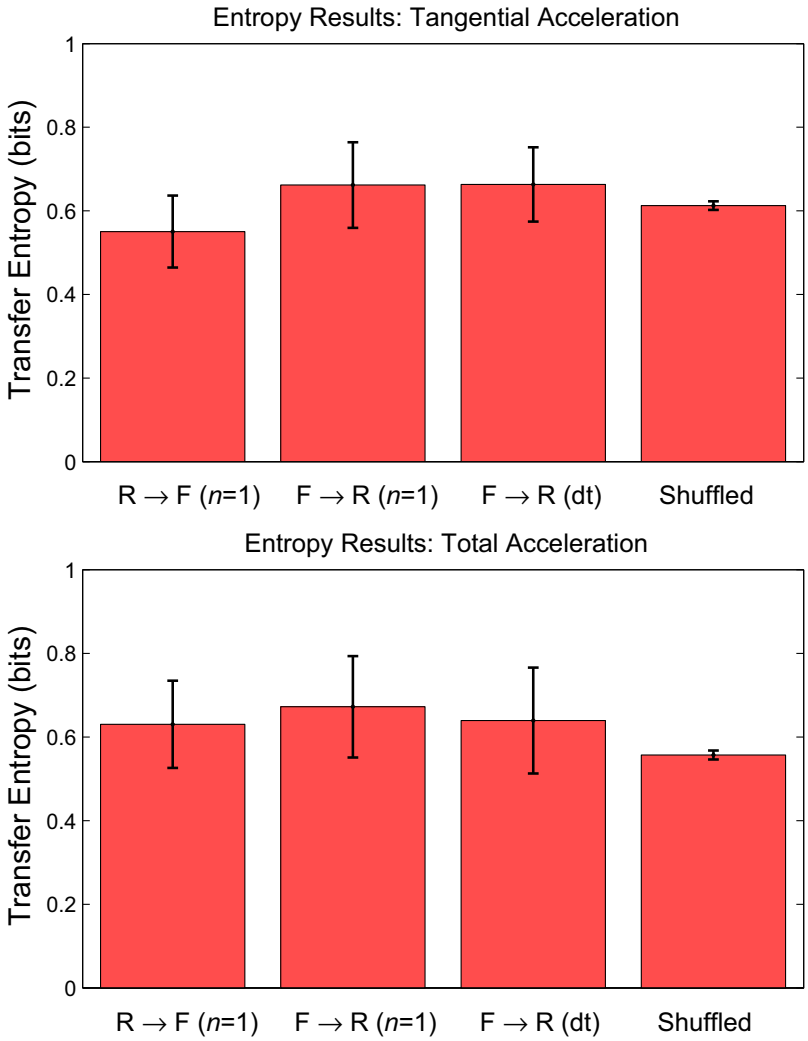

Fig. 10. Final transfer entropy results using alternative metrics. Conditions are identical those of Fig. 8: all pairs and modalities have a sample rate of 40 Hz and ten bins. Red bars represent sample means and black brackets indicate standard error. $N = 10$ pairs are used for the first three modalities and $N = 1000$ samples for the shuffled control modality.

Given the nature of transfer entropy calculations, the method employed for discretizing a continuous variable can have significant effects on the final output. In particular, results are often highly sensitive to the number of bins used to discretize. The data collection and post-processing section of this paper detailed how curvature data is discretized with a fixed logarithmic binning strategy and the transfer entropy approach and hypothesis testing section detailed the reasoning behind the choice of ten bins. Since the inter-modal trends shown in Fig. 9 are stable when we perturb the number of bins, no evidence is found that suggests the results in Fig. 8 are sensitive to the number of bins chosen.

Concerns over the accuracy of our 3D data can be addressed with the details present in the thesis describing the development of our camera system [27]. Additionally, the effects of small, or even sizable spatial inaccuracies would not have

demonstrable effects on the comparison of kinematic time series. Bats within a pair are tracked through roughly the same volume of space, so any 3D spatial error entrenched in the camera system would be present in both time series, thereby being rendered null when comparisons between the time series are made for entropy analysis.

A significant weakness of our analysis lies in the brevity of our curvature signals. The mathematics of transfer entropy creates a cardinality issue when time series of very short length are analyzed. Calculations of free information must be fed signals consisting of a sufficiently large number of points in order to properly populate all probability distributions and avoid biased results [30,37]. Though we avoid areas of highly erratic transfer entropy results by staying in timing regimes with relatively large series of points and do not see contributions from anomalous entropy calculations, it remains arguable that our curvature time series need to contain more points in order for our transfer entropy analysis to be considered reliable.

An adaptable Bayesian binning strategy [37] may provide a solution by reducing the number of bins necessary to capture the behavior of a time series, thereby reducing the cardinality and sparseness. Applying a Dirichlet distribution can reduce the effects of sparseness and regularize the probability distributions, as detailed in [30], though this can come at the cost of less significant results. More directly, an improved data collection method can serve to increase the total number of points. Expanding the tracking volume allows for an increased path length and thereby, more opportunities for interaction and information transfer, as well as a greater total number of points comprising each time series. In addition, more creative solutions may exist, such as performing cross-pair stitching to achieve representative front and rear bat signals while multiplying the total number of points. Future work with these ideas is likely to improve the validity and significance of results.

This work is supported by the National Science Foundation under grant CMMI-1342176 and by the Institute for Critical Technology and Applied Science at Virginia Tech. The authors thank Dr. J. Hanna and Dr. S.D. Ross for helpful discussions; Dr. R. Müller for providing experimental support, lab resources, and biological expertise; and the Shandong University Virginia Tech International Laboratory and its members for experimental support, expertise, and logistics.

References

1. F. Xiao, L. Wang, Int. J. Control **79**, 1277 (2006)
2. G. Dudek, M.R. Jenkin, E. Milios, D. Wilkes, Autonomous Robots **3**, 375 (1996)
3. A. Martinoli, K. Easton, W. Agassounon, The Int. J. Robotics Res. **23**, 415 (2004)
4. X.-S. Yang, Nature Inspired Cooperative Strategies for Optimization (NICSO, Springer, 2010), p. 65
5. A.R. Jordehi, Appl. Soft Computing **26**, 523 (2015)
6. N. Ulanovsky, M.B. Fenton, A. Tsoar, C. Korine, Proc. R. Soc. London B: Biol. Sci. **271**, 1467 (2004)
7. M.E. Bates, S.A. Stamper, J.A. Simmons, J. Exp. Bio. **211**, 106 (2008)
8. C. Chiu, W. Xian, C.F. Moss, Proc. Natl. Acad. Sci. **105**, 13116 (2008)
9. A.J. Corcoran, W.E. Conner, Sci. **346**, 745 (2014)
10. A. Getchell, Phys. **22**, 757 (2008)
11. F. Xiao, L. Wang, A. Wang, J. Math. Anal. Appl. **322**, 587 (2006)
12. C. Shannon, W. Weaver, *The Mathematical Theory of Information* (University of Illinois Press, 1949)
13. A. Rényi, In Fourth Berkeley Symp. Math. Stat. Probab. **1**, 547 (1961)
14. H. Marko, IEEE Trans. Commun. **21**, 1345 (1973)

15. A. Kaiser, T. Schreiber, Physica D: Nonlinear Phenomena **166**, 43 (2002)
16. T. Schreiber, Phys. Rev. Lett. **85**, 461 (2000)
17. A.G. Dimitrov, A.A. Lazar, J.D. Victor, J. Computational Neurosci. **30**, 1 (2011)
18. O. Kwon, J.-S. Yang, Phys. A: Statistical Mech. Appl. **387**, 2851 (2008)
19. G. Ver Steeg, A. Galstyan, In Proc. 21st Int. Conf. on World Wide Web, ACM, 509 (2012)
20. S. Butail, F. Ladu, D. Spinello, M. Porfiri, Entropy **16**, 1315 (2014)
21. M. Kadota, E.J. White, S. Torisawa, K. Komeyama, T. Takagi, PloS One **6**, e28241 (2011)
22. M.P. Paulus, M.A. Geyer, L.H. Gold, A.J. Mandell, Proc. Natl. Acad. Sci. **87**, 723 (1990)
23. F. Ladu, V. Mwaffo, J. Li, S. Macrì, M. Porfiri, Behav. Brain Res. **289**, 48 (2015)
24. X.R. Wang, J.M. Miller, J.T. Lizier, M. Prokopenko, L.F. Rossi, PloS One **7**, e40084 (2012)
25. J.-Y. Bouguet, Camera calibration toolbox for MATLAB, `http://www.vision.caltech.edu/bouguetj/calib_doc` (2013)
26. T. Svoboda, Multi-camera self-calibration, `http://cmp.felk.cvut.cz/~svoboda/SelfCal` (2011)
27. N. Orange, Master's thesis, Virginia Polytechnic Institute and State University (2015)
28. J.G. Puckett, D.H. Kelley, N.T. Ouellette, Scientific Reports **4** (2014)
29. M. Bergou, M. Wardetzky, S. Robinson, B. Audoly, E. Grinspun, In ACM Transactions on Graphics (TOG), ACM **27**, 63 (2008)
30. H. Choi, Neurocomputing **139**, 408 (2014)
31. D.A. Smirnov, Phys. Rev. E **87**, 042917 (2013)
32. M. Breslav, N.W. Fuller, M. Betke, In Proc. Workshop on Visual Observation and Analysis of Animal and Insect Behavior (VAIB 2012), Citeseer (2012)
33. J. Wong, D. Waters, J. Exp. Bio. **204**, 575 (2001)
34. J. Runge, J. Heitzig, N. Marwan, J. Kurths, J. Exp. Bio. **86**, 061121 (2012)
35. B.L. Ruddell, P. Kumar, Water Resources Res. **45** (2009)
36. B. Rosner, *Fundamentals of Biostatistics* (Brooks/Cole, 2011)
37. D. Endres, P. Foldiak, IEEE Trans. Information Theory **51**, 3766 (2005)